International Journal of Microwave and Wireless Technologies

cambridge.org/mrf

Beamforming steering implementation using substrate-integrated waveguide Butler matrix and slotted array antenna for 5G n257 band

Ming-An Chung, Ming-Chang Lee, Chia-Chun Hsu and Chia-Wei Lin

Department of Electronic Engineering, National Taipei University of Technology, Taipei, Taiwan

Research Paper

Cite this article: Chung MA, Lee MC, Hsu CC, Lin CW (2024) Beamforming steering implementation using substrate-integrated waveguide Butler matrix and slotted array antenna for 5G n257 band. *International Journal of Microwave and Wireless Technologies* **16**(8), 1381–1396. https://doi.org/10.1017/S1759078724001284

Received: 24 March 2024
Revised: 20 November 2024
Accepted: 22 November 2024

Keywords:
antenna array; beam switching; Butler matrix; millimeter wave; substrate-integrated waveguide

Corresponding author: Ming-An Chung; Email: mingannchung@ntut.edu.tw

Abstract

This paper introduces a method to realize beam switching by using a substrate-integrated waveguide (SIW) Butler matrix combined with a slot array antenna. The Butler matrix consists of two hybrid couplers, two crossovers, two −45-degree phase shifters, and two 0-degree phase shifters. The slot array antenna is a 4 × 2 array. The operating frequency band of the slot array antenna, where the reflection coefficient is below −10 dB, is 26.5–31.5 GHz. The measured beamforming angles from input port 1 to input Port 4 of the Butler matrix are +46, −16, +15, and −50°, respectively. The corresponding antenna gains from input Port 1 to input Port 4 are 11.57 dB, 14.284 dB, 10.94 dB, and 12.864 dB, respectively. The dimensions of the Butler matrix and the slot array antenna are 56.8 mm × 21.2 mm × 0.254 mm. The dimensions of the SIW transmission channels between the Butler matrix and input Ports 1– 4 are 16.9 mm × 34 mm × 0.254 mm.

Introduction

In recent decades, wireless communication systems have evolved from the first generation to the current fifth generation [1]. In addition, efforts are actively being made to develop the sixth generation of wireless communication systems [1]. The current fifth-generation wireless communication systems mainly utilize two frequency ranges: FR1 and FR2 [2]. FR1 operates in the frequency range of 410–7125 MHz and has been extensively utilized in various commercial and open access services, such as Zigbee, Bluetooth, Wi-Fi, GSM, CDMA, 3G, 4G, etc [3]. On the other hand, FR2 operates in the millimeter-wave frequency range of 24.25–71 GHz and offers faster transmission speeds and wider bandwidth compared to 4G [4]. The FR2 band, especially the higher frequencies, remains relatively untapped and is a focal point of attention in wireless communication [1–6].

In millimeter-wave frequency applications, one of the primary challenges is the increase in frequency, which leads to exacerbated path losses [7]. Electromagnetic waves experience more severe free-space losses and blockages, resulting in significantly reduced signal-to-interference plus noise ratio. To address this issue, many studies suggest that multiple beam antennas are a favorable solution [7–9]. The Butler matrix is one of the key beamforming networks used for this purpose. Compared to other beamforming networks, the Butler matrix offers a relatively simpler and cost-effective design, allowing for easy beam switching [10–14].

Furthermore, the Butler matrix can be implemented using microstrip technology [8, 12, 15–17], as shown in Fig. 1. A 4 × 4 Butler matrix based on microstrips typically consists of two hybrid couplers, two crossovers, and two 45-degree phase shifters. Alternatively, it can also be realized using the substrate-integrated waveguide (SIW) approach [3, 7, 11, 13, 14, 18–25].

As shown in Fig. 2, a 4 × 4 Butler matrix implemented using the SIW approach typically consists of two hybrid couplers, two crossovers, two 45-degree phase shifters, and two 0-degree phase shifters.

A comparison between Figs. 1 and 2 reveals that the microstrip-based 4 × 4 Butler matrix lacks two 0-degree phase shifters compared to the SIW-based 4 × 4 Butler matrix.

The main reason for this difference is that in the microstrip-based implementation, the hybrid coupler 2 connected to output Port 5 and hybrid coupler 4 connected to output Port 8 utilize microstrip transmission lines, which generally do not introduce phase variations. However, in the SIW-based 4 × 4 Butler matrix, to ensure phase consistency, 0-degree phase shifters are used to connect hybrid coupler 2 with output Port 5 and hybrid coupler 4 with output Port 8 [13]. However, the application of a 4 × 4 Butler matrix in SIW form at millimeter-wave frequencies is prone to significant dielectric loss, leading to reduced radiation efficiency. Consequently, some studies have explored using a Coplanar waveguide (CPW)-type Butler matrix to address this issue [26]. Nevertheless,

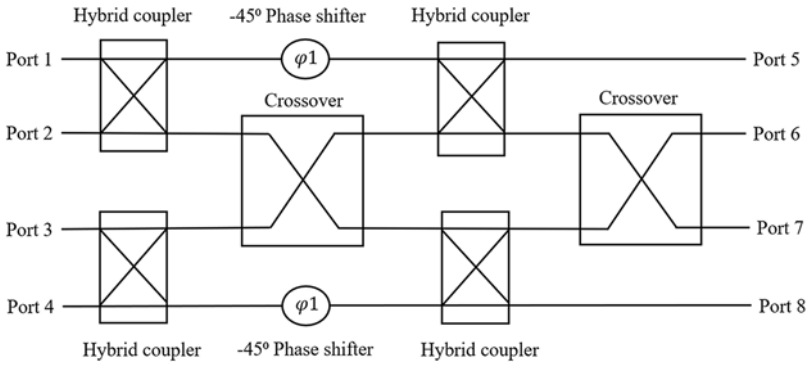

Figure 1. 4 × 4 Butler matrix in the form of microstrip lines.

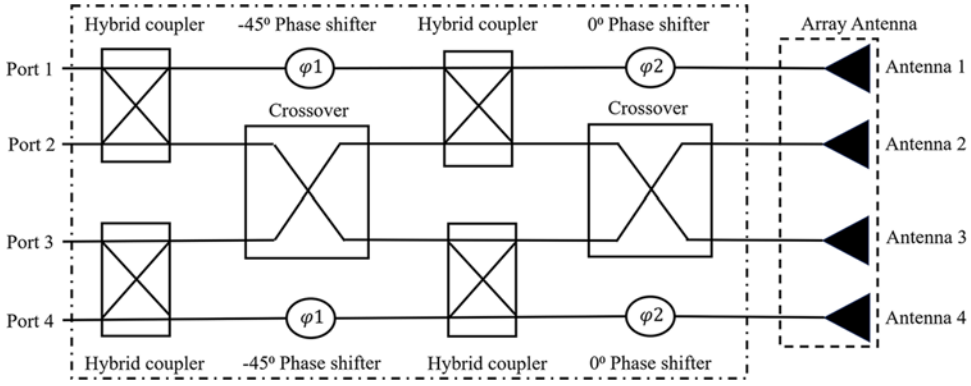

Figure 2. SIW-based 4 × 4 Butler matrix combined with an array antenna.

it is evident that the periphery of the CPW-type Butler matrix still involves SIW design, which increases the complexity of the overall design.

In fact, there have been many studies aimed at reducing antenna size by designing three-dimensional or multilayer structures for the Butler matrix [19–21]. However, this approach significantly increases the complexity of the design [13], and it does not necessarily guarantee an improvement in antenna gain, thus not fully exploiting the characteristics of the Butler matrix.

Due to the need for multiple 0-degree phase shifters in the SIW-based 4 × 4 Butler matrix design, it is relatively more complex compared to the microstrip-based 4 × 4 Butler matrix. However, the SIW-based 4 × 4 Butler matrix offers the advantage of low loss and, when combined with a slotted array antenna designed using SIW, further enhances antenna gain [13].

Despite extensive research on microstrip-based and SIW-based Butler matrices for beamforming in millimeter-wave applications, significant challenges remain, particularly concerning dielectric losses in SIW designs and the complexity of multilayer structures. Additionally, prior designs have exhibited limitations in antenna gain and bandwidth coverage, necessitating further investigation to improve performance for 5G n257 bands.

In this paper, a SIW Butler matrix slot array antenna is proposed. This proposed antenna exhibits good antenna gain (10.94 ∼ 14.284 dB) and features a planar single-layer structure. By adjusting the positions of the metal vias inward or adding an additional row of metal vias inside the existing metal vias without expanding the outer dimensions, the design addresses the issue of excessive dielectric loss leading to reduced radiation. This approach simplifies the structure and makes it easy to fabricate while maintaining good antenna gain. In the "Brief theory of Butler matrix" section, a brief introduction to the theoretical aspects of the Butler matrix is provided, followed by the design process of various components of the Butler matrix in the "Butler matrix design process" section. The "Simulation of the Butler matrix" section presents the simulation of the Butler matrix, while the "Measurement and comparison of the Butler matrix antenna" section presents the measurement results and compares the contributions of this study. Finally, the "Conclusion" section offers conclusions and outlines future directions for improvement.

In this paper, we propose a novel SIW-based Butler matrix design that overcomes the aforementioned challenges by incorporating inward-positioned metal vias and additional rows of vias within the existing structure. This approach minimizes dielectric loss and enhances antenna gain while maintaining a planar, single-layer design. Such an innovation simplifies fabrication and reduces manufacturing costs, making it more feasible for large-scale production and practical 5G applications.

Unlike previous designs that employ multilayer or CPW-based Butler matrices [7, 8, 11–24, 26], which tend to suffer from increased complexity and dielectric losses, our design utilizes a single-layer SIW approach with tailored metal via positioning to enhance performance. Compared to other designs, our proposed Butler matrix demonstrates a more favorable trade-off between gain and simplicity.

The main contributions of this study are as follows:

(1) a novel design approach using inward-positioned metal vias for improved gain and reduced dielectric loss;
(2) a single-layer, planar structure that simplifies the overall design while maintaining robust beamforming capabilities;

https://doi.org/10.1017/S1759078724001284 Published online by Cambridge University Press

(3) a comprehensive comparison with existing designs, demonstrating superior bandwidth coverage and ease of fabrication for 5G n257 band applications.

Brief theory of Butler matrix

According to the SIW Butler matrix shown in Fig. 2, it consists of two hybrid couplers, two crossovers, two −45-degree phase shifters and two 0-degree phase shifters. The Butler matrix will be connected to an antenna array, forming a multi-beam antenna as shown in Fig. 1. The direction of rotation of the beam can be calculated using Formula 1 [13].

$$\theta_{\text{direction}} = 90^{\circ} - \cos^{-1}\left(\frac{\lambda\phi}{2\pi d}\right), -90^{\circ} \leqslant \theta_{\text{direction}} \leqslant 90^{\circ} \quad (1)$$

where λ represents the wavelength, d is the distance between two adjacent elements (usually equal to or less than λ/2), and φ is the phase difference between any two adjacent antennas in the array. The beam steering direction is achieved through the phase difference between neighboring antennas, and the phase difference between antennas is controlled by the Butler matrix.

Butler matrix design process

In this paper, the Butler matrix is simulated and designed using a Rogers Duriod 5880 substrate, with a loss tangent of 0.0009 and a relative dielectric constant of 2.2. The phase differences between consecutive antennas are set at −45°, 135°, −135°, and 45°, resulting in theoretical beam angles of 14.4°, −48.6°, 48.6°, and −14.4°, respectively.

According to the structural characteristics of the SIW-based Butler matrix, the cross-coupler is formed by connecting two hybrid couplers together, and the size and structure of the phase shifter are constrained by the hybrid coupler and crossover. As a result, the size of the hybrid coupler determines the overall size of the Butler matrix in this study. Additionally, since the phase shifter needs to change phase, a straight-line structure is not feasible, and a bending structure is required for its implementation. However, in the proposed Butler matrix, to avoid increasing its size, the phase shifter's structure is positioned toward the overall center, preventing the matrix from expanding its dimensions outward.

Hybrid coupler

To achieve desired phase differences of −45°, 135°, −135°, and 45° between consecutive antennas, a hybrid coupler with a phase difference of −90° is used in this study. The hybrid coupler utilizes metal via holes with a size of 0.4 mm and a spacing of 0.8 mm between adjacent metal via holes. The dimensions and geometry of the designed hybrid coupler are shown in Fig. 3 and Table 1.

In this study, the required frequency band, reflection loss, transmission coefficient, and output phase difference are achieved by adjusting the length, width, and position of the metal vias in the hybrid coupler. For instance, shifting the entire row of L5 metal vias horizontally by 0.4 mm toward Ports 1 and 2 increases the frequency of the hybrid coupler, resulting in a phase difference of −270°. Conversely, shifting the vias 0.4 mm toward Ports 3 and 4 decreases the frequency, resulting in a phase difference of +90°. The frequency of the proposed hybrid coupler lies between these two scenarios, maintaining a phase difference of −90°, as shown in Figs. 4 and 5. This demonstrates that adjusting the position of the metal vias is crucial for meeting the design requirements of the hybrid coupler.

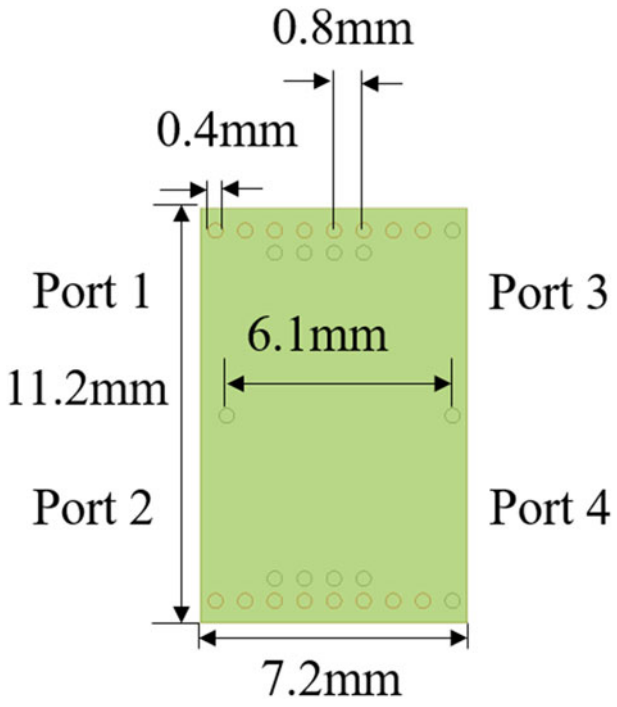

Figure 3. Schematic diagram of the dimensions of the hybrid coupler.

Table 1. Hybrid coupler dimensions

Parameter	Value (mm)	Parameter	Value (mm)
L	7.2	W	11.2
l_1	0.8	w_1	0.6
l_2	0.4	w_2	5.6
l_3	0.8	w_3	0.6
l_4	6.1		
l_5	0.4		

Figure 4 shows that the reflection coefficient S11 and isolation S21 of the proposed hybrid coupler are below −10 dB in the frequency range of 25–37.5 GHz. When the frequency of the proposed hybrid coupler is 28 GHz, the through Port S31 is −2.63 dB, and the coupled Port S41 is −4.13 dB, as depicted in Fig. 5. The phase difference between Port 1 and Port 3 is approximately −90.7°.

Crossover

The structure of the cross-coupler in this paper is slightly modified from the typical configuration, where two hybrid couplers are connected in series. In the modified design, the last metal via hole of the first hybrid coupler is shared with the first metal via hole of the second hybrid coupler, as shown in Fig. 6. This approach helps to slightly reduce the size of the cross-coupler.

https://doi.org/10.1017/S1759078724001284 Published online by Cambridge University Press

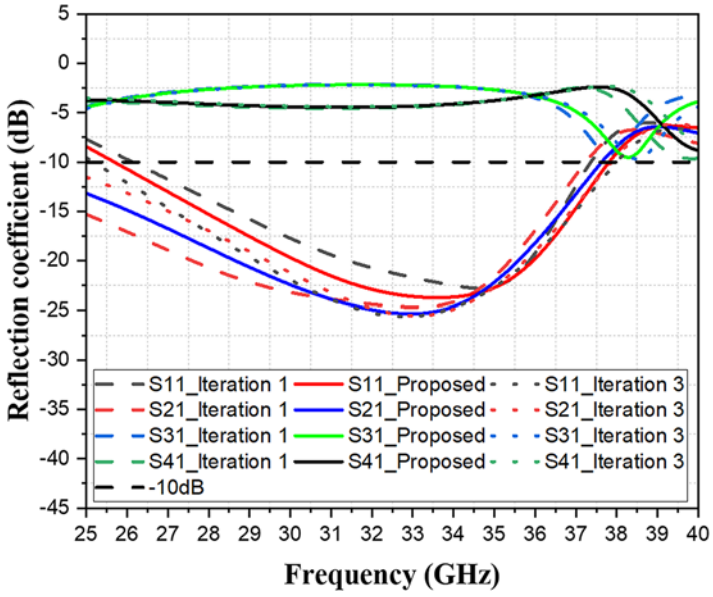

Figure 4. Simulated S-parameter of the hybrid coupler.

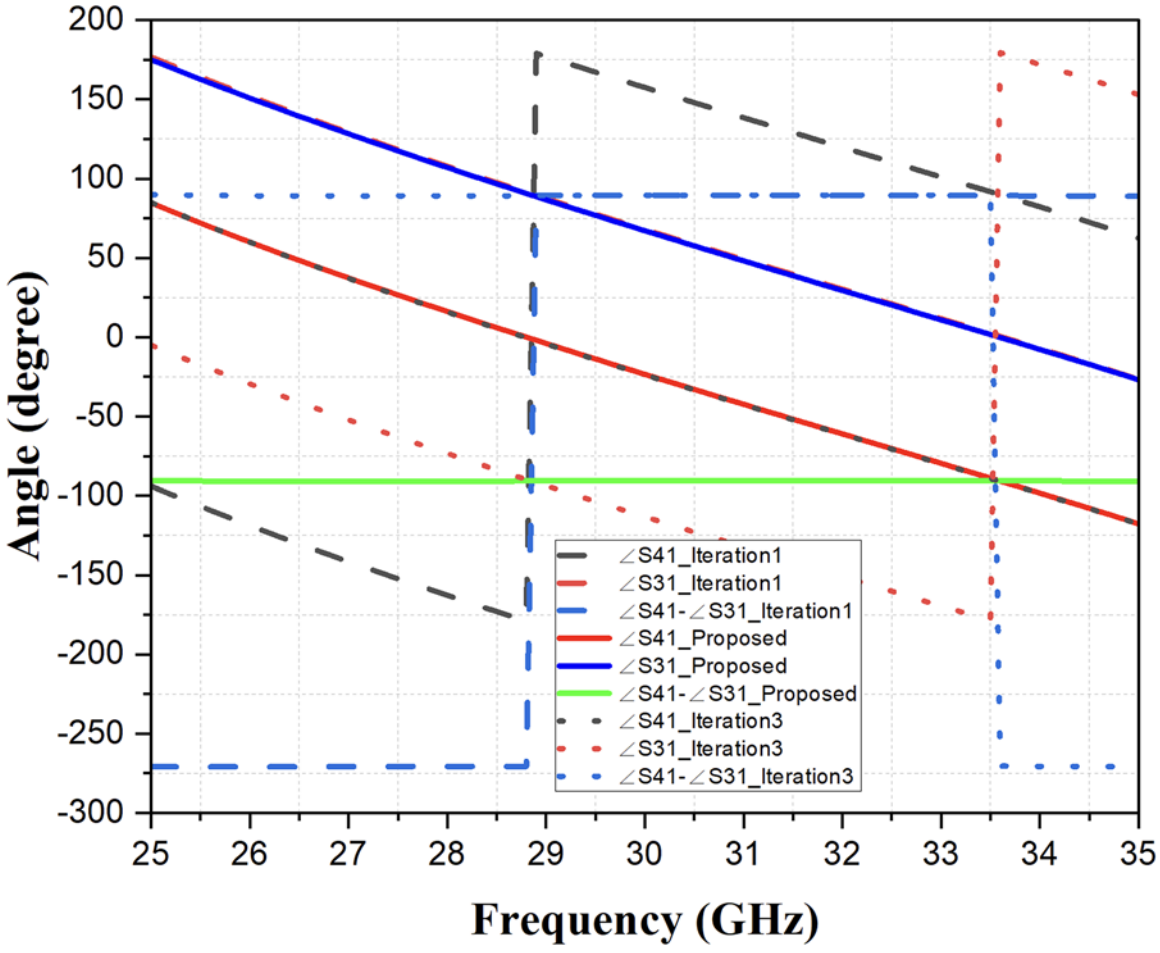

Figure 5. Schematic diagram of the phase difference between S31 and S41 for the hybrid coupler.

Figure 7 presents the simulation results, indicating that the reflection coefficient S11 and isolation levels S21 and the crossover Port S31 are all below −10 dB in the frequency range of 26–33 GHz. At 28 GHz, through Port S41 is −0.47 dB. These simulation results demonstrate that the cross-coupler meets the design requirements.

https://doi.org/10.1017/S1759078724001284 Published online by Cambridge University Press

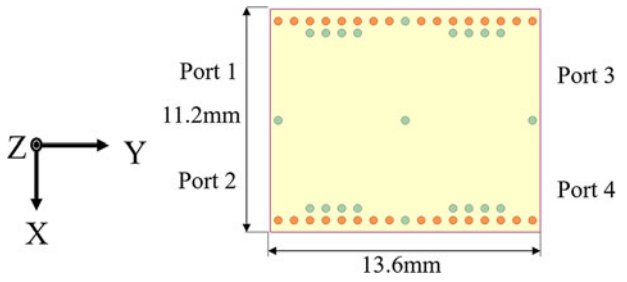

Figure 6. The cross-coupler dimensions.

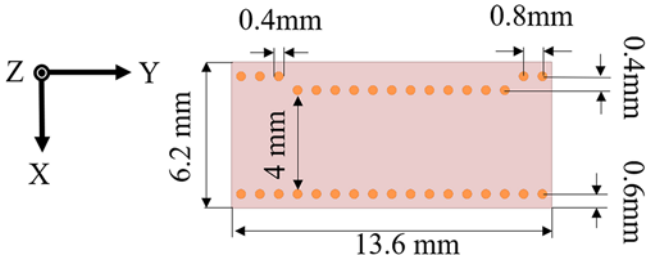

Figure 7. Simulated S-parameter of the crossover.

Phase shifter

The phase shifter is a critical component in the Butler matrix, used in conjunction with the phase difference of the hybrid coupler to achieve fixed output phase shifts. In this design, the hybrid coupler has a phase difference of −90°, so the required corresponding phase shifters are −45° and 0°. The size of the phase shifter is constrained by the dimensions of the hybrid and crossover and cannot be adjusted by altering the length or width of the substrate.

Additionally, the inner side of the phase shifter shares one side of the metal via holes with the cross-coupler, making it impossible to change the position of the inner metal via holes.

Several studies have suggested different approaches to design the phase shifter, such as bending the outer row of metal via holes outward or inserting multiple metal via holes internally. However, bending the metal via holes outward would increase the overall size of the structure and adding additional metal via holes would introduce additional fabrication costs and time. In this paper, without increasing the overall size or using additional metal via holes, the approach of moving the positions of the outer metal via holes of the phase shifter inward is adopted to achieve the design of the −45-degree and 0-degree phase shifters.

−45-degree phase shifter

The structure of the −45-degrees phase shifter has the same length as the cross-coupler and a width equal to the size of the hybrid couplers it connects to. The overall size of the −45-degrees phase shifter is depicted in Fig. 8.

As shown in Fig. 9, the simulation results indicate that the reflection coefficient (S11) of the −45-degrees phase shifter is below −10 dB in the frequency range of 25–35 GHz. At 28 GHz, the transmission coefficient (S21) is −0.24 dB, as depicted in Fig. 9. Furthermore, at 28 GHz in Fig. 10, the phase shift is simulated to be −44.28°, confirming that the −45-degree phase shifter meets the design requirements.

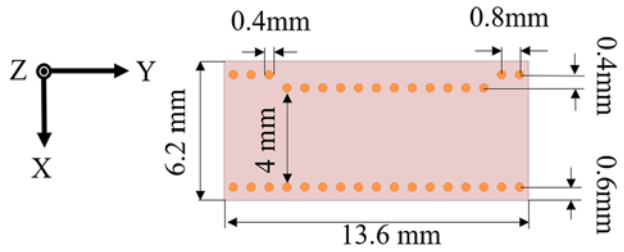

Figure 8. Dimensions diagram of the −45-degree phase shifter.

0-degree phase shifter

The structure of the 0-degree phase shifter is designed under the same constraints as the 45-degree phase shifter. Therefore, the same design approach as used for the 45-degree phase shifter to implement the 0-degree phase shifter. The overall size of the 0-degree phase shifter is shown in Fig. 11.

As depicted in Fig. 12, the simulation results demonstrate that the reflection coefficient (S11) of the 0-degree phase shifter is below −10 dB in the frequency range of 25–35 GHz. At 28 GHz, the transmission coefficient (S21) is −0.24 dB, as shown in Fig. 12. Moreover, at 28 GHz in Fig. 13, the phase shift is simulated to be −0.23°, which is very close to 0°. These simulation results confirm that the 0-degree phase shifter meets the design requirements.

Slot antenna

Slot antennas have been widely used in SIW-form Butler matrices, and their design typically involves a size of about half a wavelength. This allows for smaller antenna dimensions and extends the SIW's structure, increasing the isolation between adjacent antenna elements. Moreover, when the adjacent antenna elements are spaced half a wavelength apart, the radiated electromagnetic waves can be aggregated, leading to an increase in antenna gain.

In this paper, the design of the Butler matrix took the requirements of the slot antennas into consideration before designing the hybrid coupler. In other words, the slot antenna was the first element to be considered and designed in this study. The structure and dimensions of the antenna slot used in this article are depicted in Fig. 14 and Table 2.

As shown in Fig. 15, the simulation results of this slot antenna indicate that the reflection coefficient is below −10 dB in the frequency ranges of 27.55–28.75 GHz, 30.78–31.32 GHz, and 34.65–35.28 GHz.

The proposed slot antenna was simulated with input phase settings of −45, −90, −135, and −180° for Ant. 1, Ant. 2, Ant. 3, and Ant. 4, respectively, to form a beam angle of +14° and a gain of 12.94 dB at the frequency of 28 GHz.

Similarly, for Port 2, the input phase settings were set to −135°, −0°, −225°, and −90° for Ant. 1, Ant. 2, Ant. 3, and Ant. 4, respectively, resulting in a beam angle of −48° and a gain of 13.76 dB at a frequency of 28 GHz.

For Port 3, the input phase settings were −90°, −225°, −0°, and −135° for Ant. 1, Ant. 2, Ant. 3, and Ant. 4, respectively, to achieve a beam angle of 47° and a gain of 13.24 dB at the frequency of 28 GHz.

Finally, for Port 4, the input phase settings were −180°, −135°, −90°, and −45° for Ant. 1, Ant. 2, Ant. 3, and Ant. 4, respectively, resulting in a beam angle of −15° and a gain of 13.26 dB at

https://doi.org/10.1017/S1759078724001284 Published online by Cambridge University Press

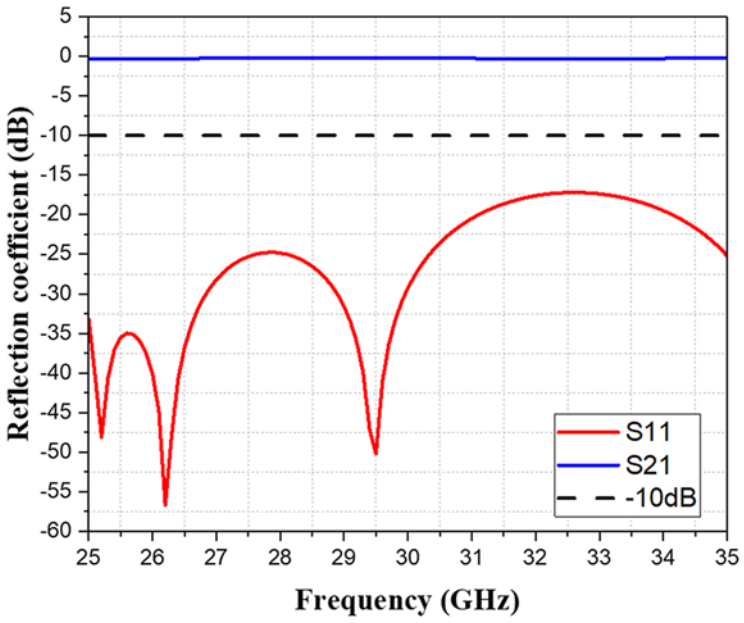

Figure 9. Simulated S-parameter of −45-degree phase shifter.

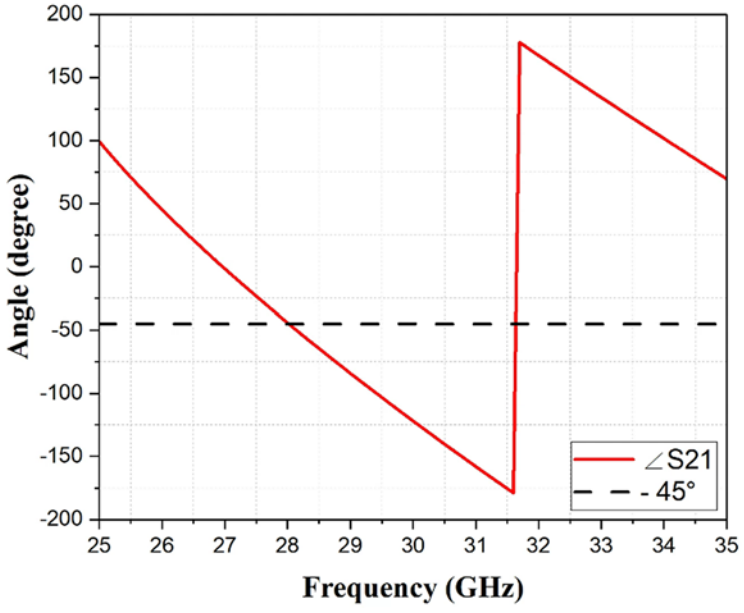

Figure 10. The phase of a −45-degree phase shifter.

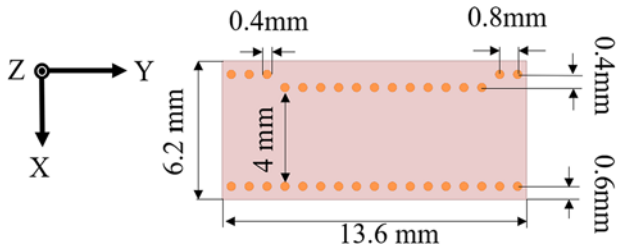

Figure 11. Dimensions of a 0-degree phase shifter.

https://doi.org/10.1017/S1759078724001284 Published online by Cambridge University Press

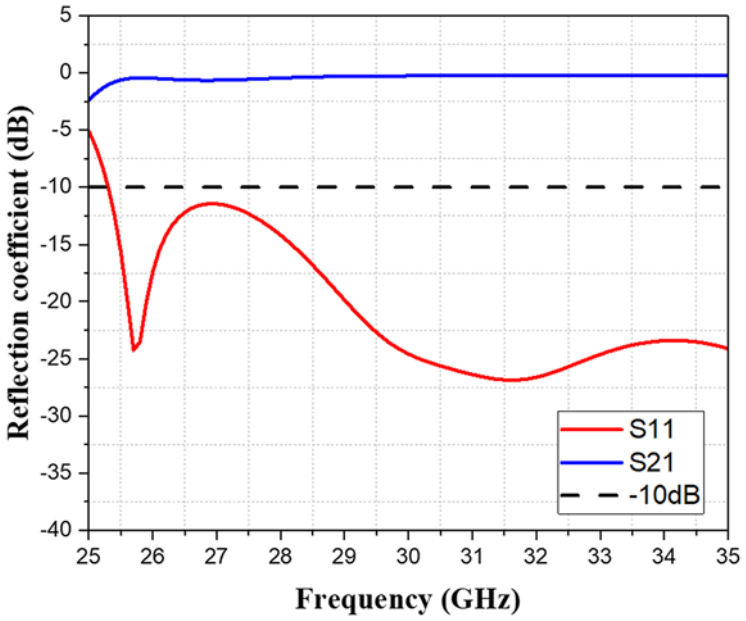

Figure 12. Simulated S-parameter of 0-degree phase shifter.

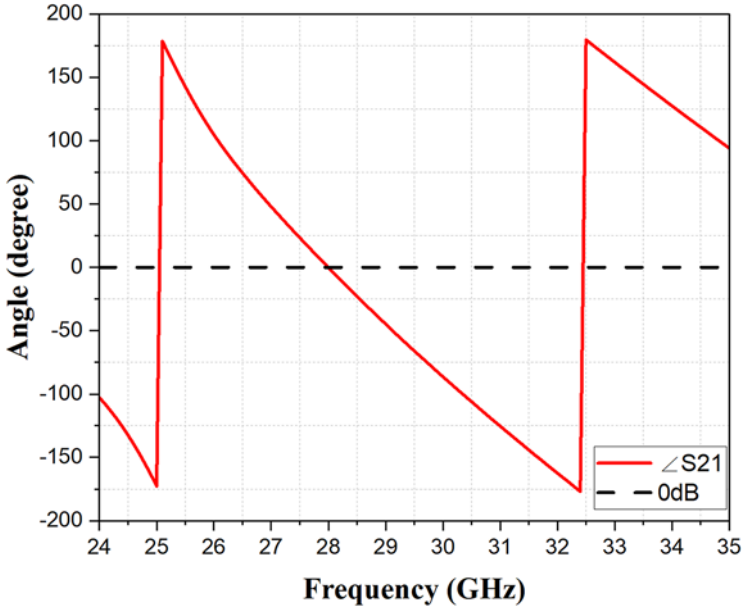

Figure 13. The phase of a 0-degree phase shifter.

the frequency of 28 GHz. The simulation results are illustrated in Fig. 16.

Although this slotted antenna design has a narrower bandwidth and does not meet the 5G n257 band, the gain of this slotted antenna is significantly higher than that of some other slotted antenna designs reported in the reference [27]. Additionally, the final antenna bandwidth can be adjusted to cover the 5G n257 band by tuning the SIW transmission channel, as discussed later.

Simulation of the Butler matrix

In this section, the previously designed hybrid couplers, crossovers, 45-degree phase shifter, and 0-degree phase shifter, each with their respective dimensions and configurations as described earlier, have been successfully combined following the structure shown in Fig. 1. The same metal via is used between adjacent elements, with the first metal via of the preceding element connected to the last metal via of the subsequent element. The size and spacing of the metal vias are maintained as in the original design to ensure phase consistency and proper transmission. The general dimensions of the combined Butler matrix are shown in Fig. 17.

In Fig. 17, the Butler matrix shows a symmetric structure between Port 1 and Port 4, as well as between Port 2 and Port 3. As indicated in the simulation results, the trend of the reflection coefficients S11 and S44 for Port 1 and Port 4 is highly consistent. Similarly, the trend of reflection coefficients S22 and S33 for Port 2 and Port 3 is also in close agreement, reflecting the mutual correspondence between Port 1 and Port 4, and Port 2 and Port 3 due

https://doi.org/10.1017/S1759078724001284 Published online by Cambridge University Press

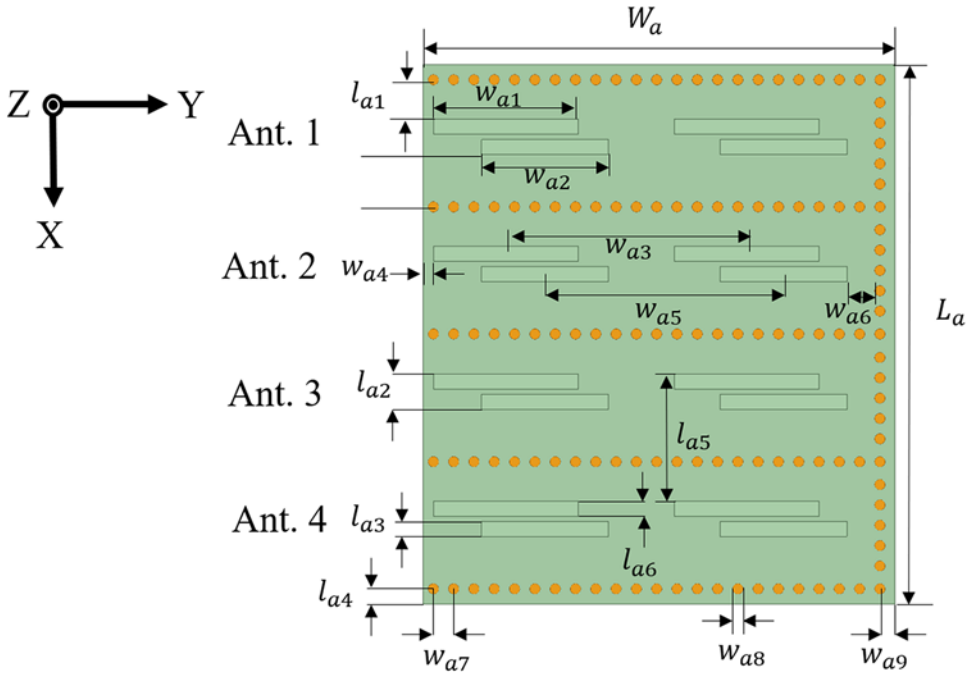

Figure 14. The dimensions of the SIW slot antenna.

Table 2. SIW slot antenna dimensions

Parameter	Value (mm)	Parameter	Value (mm)
L_a	21.2	W_a	18.6
l_{a1}	1.35	w_{a1}	5.7
l_{a2}	1.39	w_{a2}	5
l_{a3}	0.59	w_{a3}	9.5
l_{a4}	0.6	w_{a4}	0.7
l_{a5}	5	w_{a5}	9.4
l_{a6}	0.6	w_{a6}	1.1
		w_{a7}	0.8
		w_{a8}	0.4
		w_{a9}	0.6

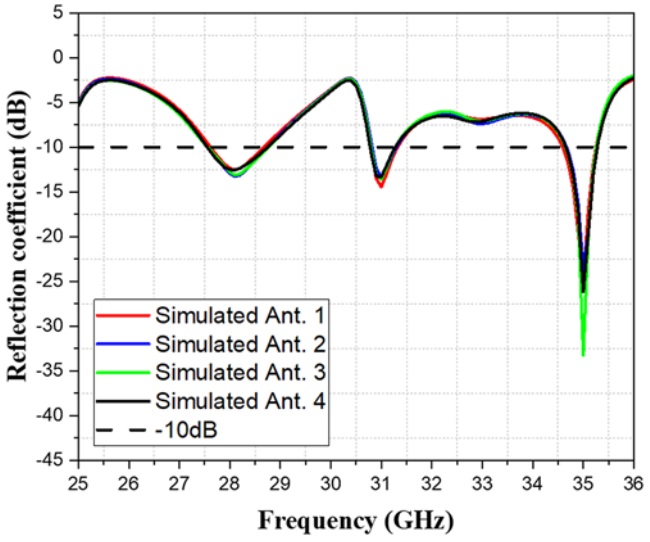

Figure 15. The reflection coefficient of the slot antenna.

to their symmetric configuration. Moreover, the reflection coefficient S11 for Port 1 remains below −10 dB in the frequency range of 26.67–34.73 GHz, while the reflection coefficient S44 for Port 4 remains below −10 dB in the frequency range of 26.61–33.63 GHz, as shown in Fig. 18.

As shown in Fig. 19, the final design resulted in reflection losses of −10 dB or below at a frequency of 28 GHz when Ports 1–4 were excited, using the original Butler matrix combined slot antenna and 1.85 mm coaxial connectors, along with the adjusted positions of the metal via holes in the SIW transmission channel.

Figure 20 illustrates the frequency ranges for Ports 1– 4, where Port 1 operates in the frequency range of 26.4 –32.52 GHz, Port 2 in the range of 27.1–30.56 GHz, Port 3 in the range of 27.1–30.56 GHz, and Port 4 in the range of 27.12–30.56 GHz.

Figure 21 presents the performance results when each Port (Port 1–4) is individually excited. At a frequency of 28 GHz, Port 1 achieved a maximum gain of 10.57 dB with a beam angle of 44°. Port 2 demonstrated a maximum gain of 10.56 dB and a beam angle of −19°. Port 3 exhibited a maximum gain of 10.34 dB with a beam angle of 19°. Finally, Port 4 showed a maximum gain of 11.35 dB with a beam angle of −43°. These results closely align with the theoretical beam angles for Ports 1–4.

Furthermore, as shown in Fig. 22, this study also explored the original Butler matrix combined slot antenna with end launch coaxial connectors and adjusted the positions of the metal via holes in the SIW transmission channel to reduce transmission losses. The goal was to maintain the correct beam angles when Ports 1–4 were excited and achieve reflection losses of −10 dB or lower at a frequency of 28 GHz, and even extend the reflection losses to cover the n257 frequency band. Furthermore, as shown in Fig. 22,

https://doi.org/10.1017/S1759078724001284 Published online by Cambridge University Press

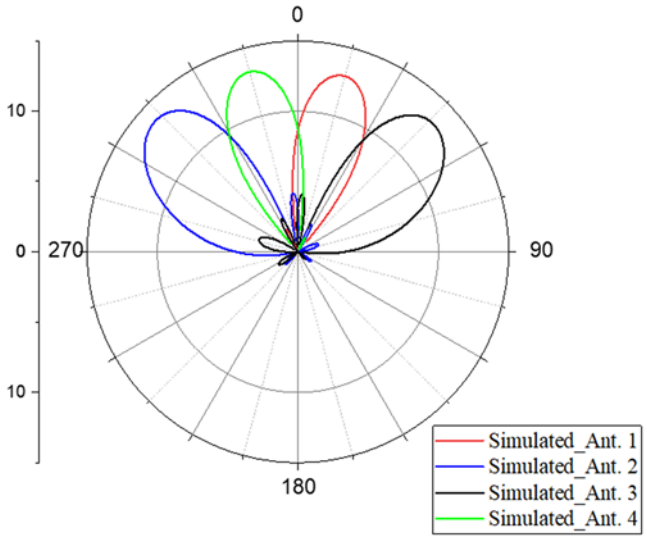

Figure 16. The beam angle and gain of the proposed slot antenna for analogue Ports 1–4 at 28 GHz.

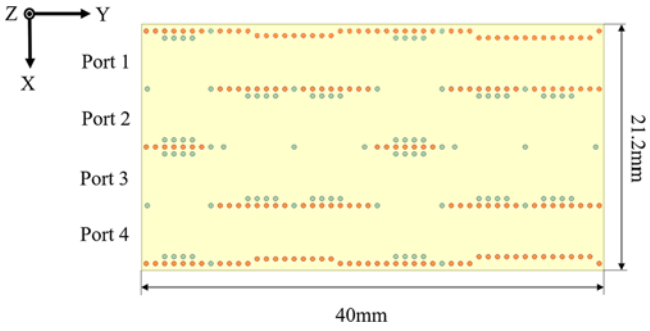

Figure 17. The dimensions of the Butler matrix.

this study also explored the original Butler matrix combined slot antenna with end launch coaxial connectors and adjusted the positions of the metal via holes in the SIW transmission channel to reduce transmission losses. The goal was to maintain the correct beam angles when Ports 1– 4 were excited and achieve reflection losses of −10 dB or lower at a frequency of 28 GHz, and even extend the reflection losses to cover the n257 frequency band.

Figure 26 illustrates the frequency ranges for Ports 1– 4, where Port 1 operates in the frequency range of 27.3–32.5 GHz, Port 2 in the range of 26.65– 30.3 GHz, Port 3 in the range of 26.6–30.3 GHz, and Port 4 in the range of 27.3–32.5 GHz.

Figure 28 presents the performance results when each Port (Port 1–4) is individually excited. At a frequency of 28 GHz, Port 1 achieved a maximum gain of 10.8 dB with a beam angle of 48°. Port 2 demonstrated a maximum gain of 9.85 dB and a beam angle of −19°. Port 3 exhibited a maximum gain of 10.4 dB with a beam angle of 19°. Finally, Port 4 displayed a maximum gain of 10.27 dB with a beam angle of −39°. Although the beam angle for Port 4 differed by 6° from the theoretical value, the original Butler matrix combined slot antenna with end launch coaxial connectors offered better bandwidth. Consequently, this design was selected for subsequent measurements.

Measurement and comparison of the Butler matrix antenna

The proposed Butler matrix array antenna was manufactured and measured as shown in Fig. 23, with overall dimensions identical to those depicted in Fig. 22. The measurements were made using a Keysight N5293A network analyzer, and Fig. 24 provides a photograph of the measured reflection losses.

For measuring antenna gain and radiation patterns, an Atenlab R3 anechoic chamber was used. Figure 25 presents a photograph of the measurement setup for the radiation patterns and gain. During the measurement process, all ports (Port 1–Port 4) were connected using end launch coaxial connectors.

As shown in Fig. 26, the results of the reflection coefficient measurement for the sample of the Butler matrix array antenna indicate that they are below −10 dB. The frequency ranges for each port are as follows:

Port 1 operates in the range of 26.8–31.8 GHz.

Port 2 operates in the range of 25.8–32.8 GHz.

Port 3 operates in the range of 25.8–31.4 GHz. The reflection loss of Port 3 is slightly higher than −10 dB in the frequency range of 29.8–30.5 GHz.

Port 4 operates in the frequency range of 26.8–31.8 GHz.

Figure 27 presents the measured gain results for Ports 1– 4 of the Butler matrix array antenna sample at a frequency of 28 GHz. The gains are as follows: Port 1-11.57 dB, Port 2-14.28 dB, Port 3-11.94 dB, and Port 4-12.84 dB. Additionally, the maximum gains at the frequency point of 28 GHz are: Port 1-15.71 dB, Port 2-17.848 dB, Port 3-14.02 dB, and Port 4-14.96 dB.

As shown in Fig. 28, at a frequency of 28 GHz, the measured beam angles for the sample antenna were as follows:

Port 1 had a beam angle of 44°.
Port 2 had a beam angle of −14°.
Port 3 had a beam angle of 15°.
Port 4 had a beam angle of −50°.

In Fig. 28, the discrepancy between the measured and simulated gains, where the measured gain is significantly higher, can be attributed to two main factors: differences in the testing environment and manufacturing tolerances.

Firstly, testing environment differences can lead to variations in measured results, as real-world testing conditions may introduce reflections or interference that are not accounted for in the simulation model. These external influences can enhance the measured gain, creating a discrepancy when compared to idealized simulation results.

Secondly, manufacturing tolerances can also impact the antenna's performance. Minor variations in the fabrication process, such as slight deviations in component dimensions or material properties, can affect the antenna's gain characteristics. These tolerances may lead to improved gain in the measured prototype compared to the theoretical model used in simulations.

The azimuth plane beam coverage at a frequency of 28 GHz is depicted in Fig. 29. After normalizing the antenna gains of Ports 1–4, the beam coverage range is more prominently shown to be between −50° and 44°, as illustrated in Fig. 29.

The comparison between simulation and measurement results reveals that the beam angles of Ports 1– 3 in the sample antenna differ by approximately 4°, while Port 4's beam angle differs by 11°. Additionally, the measured frequency ranges for Ports 1–4

https://doi.org/10.1017/S1759078724001284 Published online by Cambridge University Press

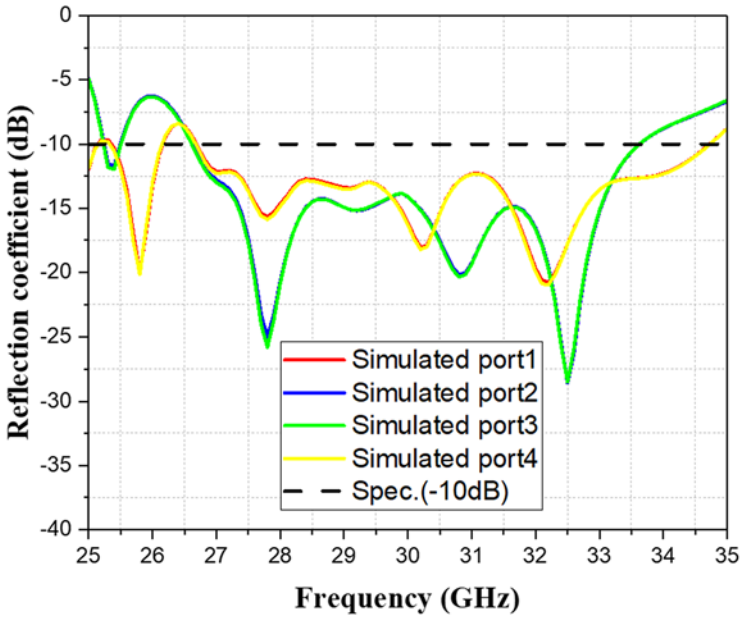

Figure 18. The reflection coefficient of the Butler matrix.

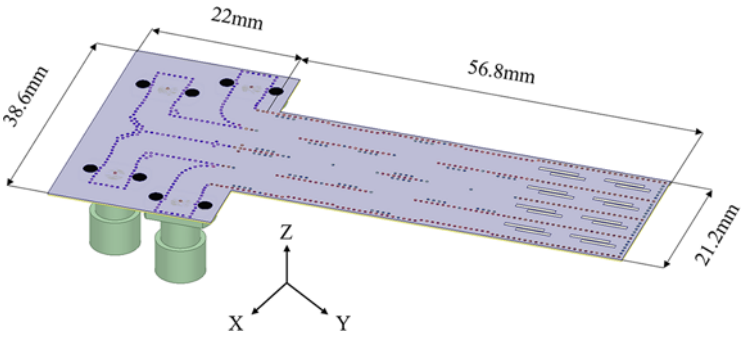

Figure 19. The Butler matrix combined the slot antenna with the adjusted SIW transmission channel and 1.85 mm coaxial connectors.

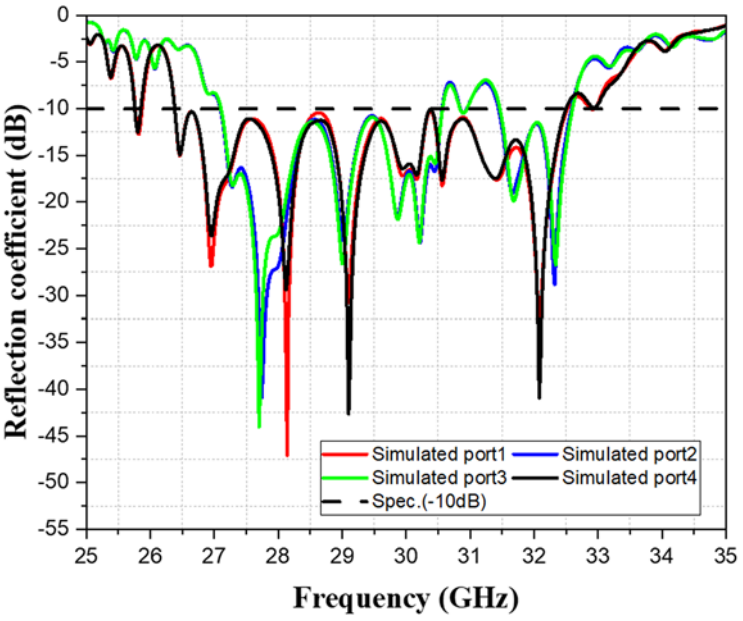

Figure 20. The schematic diagram of the reflection coefficient for Ports 1–4 after excitation is shown in Figure 19.

https://doi.org/10.1017/S1759078724001284 Published online by Cambridge University Press

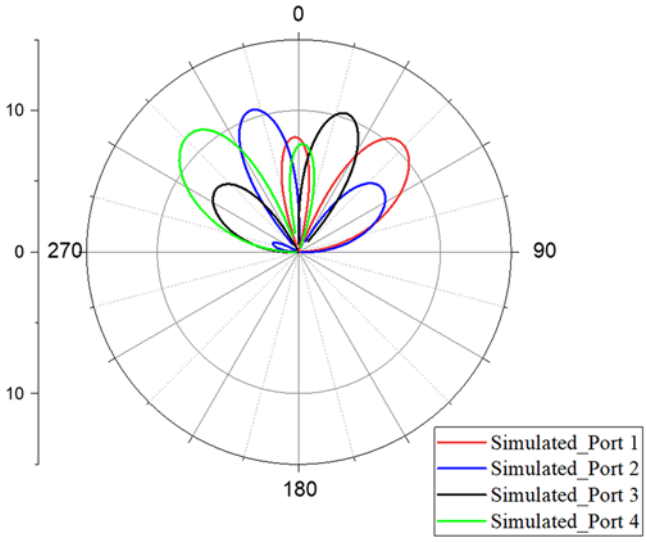

Figure 21. The beam angle schematic diagram for Ports 1– 4 after excitation in Figure 19.

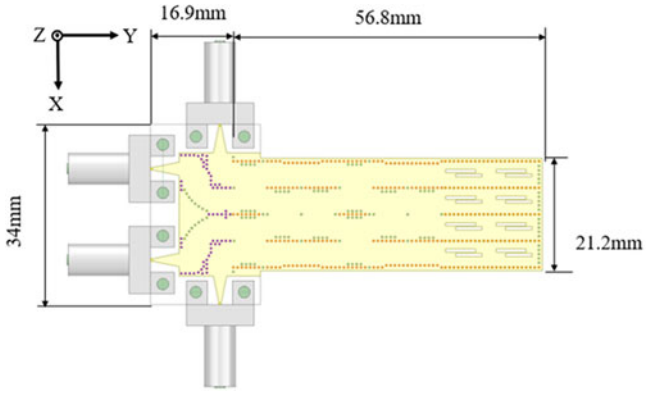

Figure 22. The original Butler matrix combined the slot antenna with the adjusted SIW transmission channel and the end-launch coaxial connectors.

show a slight increase, which may be attributed to manufacturing discrepancies.

Discussion and comparison

In this paper, similar studies are compared with the proposed design in Table 3. The comparison highlights several advantages of the design presented in this study. First, the sample from this work covers a frequency range of approximately 26–32 GHz, offering a competitive bandwidth that is comparable to or wider than other single-layer and multilayer designs listed in Table 3. For instance, the bandwidth of the proposed design is wider than those reported in references [7–19, 21–24] [12], and comparable to multilayer designs such as [20].

Second, the size of the proposed antenna (56.8 × 21.2 mm) is relatively compact, particularly when compared to multilayer designs like [18–21, 23, 24], which have a significantly larger footprint, which also has larger dimensions. This compact size, combined with the single-layer structure, makes the proposed design well-suited for practical applications requiring miniaturization.

In terms of peak gain, while the gain of the sample (14.28 dB) is slightly lower than those reported in references [19] (14.37 dB) and [20] (15.81 dB), it still performs competitively. It surpasses the gain achieved by several other single-layer designs, such as references [12] (6.7 dB) and [11] (10.2 dB), demonstrating the effectiveness of the inward-positioned metal vias in enhancing performance without increasing the complexity.

Moreover, the single-layer design presented in this work offers advantages in terms of fabrication simplicity and cost-efficiency, as it avoids the increased complexity and potential dielectric losses associated with multilayer and CPW-based designs, such as those in references [16, 18], and [22]. This design choice

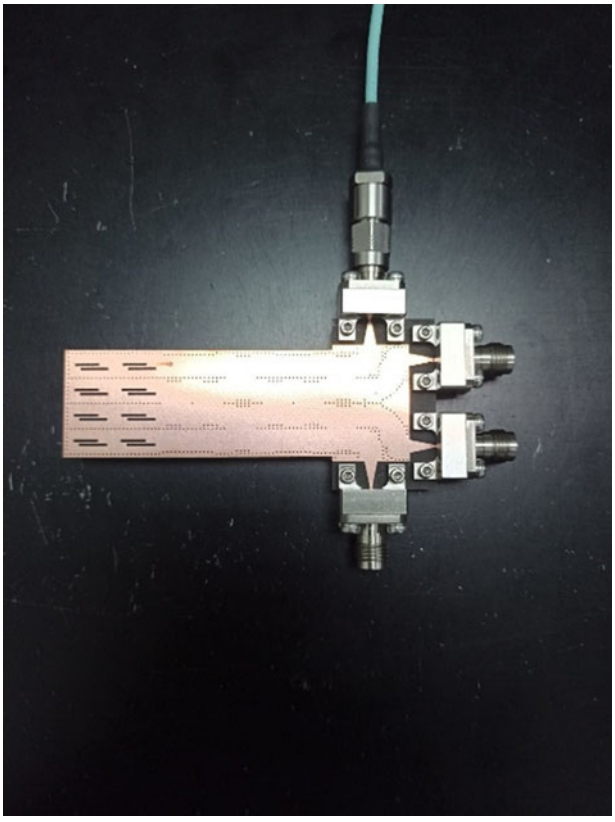

Figure 23. The fabricated sample of the Butler matrix antenna with the end-launch coaxial connectors connected.

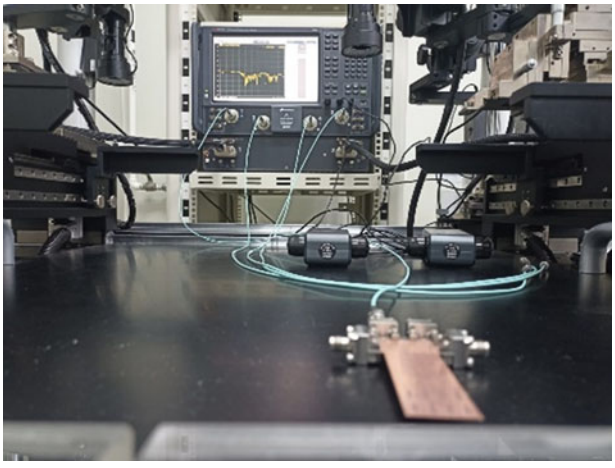

Figure 24. Measurement of the reflection coefficients of the Butler matrix antenna sample.

https://doi.org/10.1017/S1759078724001284 Published online by Cambridge University Press

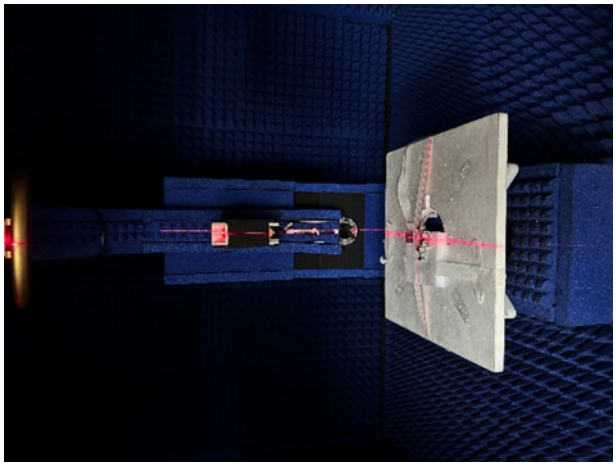

Figure 25. Measurement of radiation patterns and gain of the Butler matrix antenna sample.

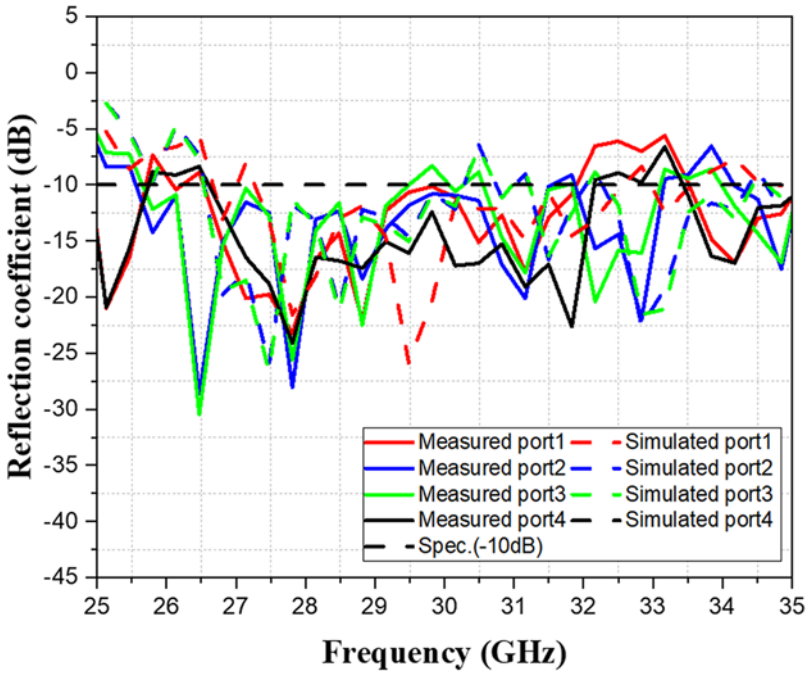

Figure 26. Measured and simulated reflection loss of the Butler matrix antenna.

enhances its suitability for large-scale production and commercial applications.

Overall, the results indicate that the proposed design exhibits favorable characteristics, including broader bandwidth, compact size, and competitive gain, when compared to other research designs. The single-layer structure further enhances the feasibility of this design for mass production and potential integration into commercial 5G systems.

https://doi.org/10.1017/S1759078724001284 Published online by Cambridge University Press

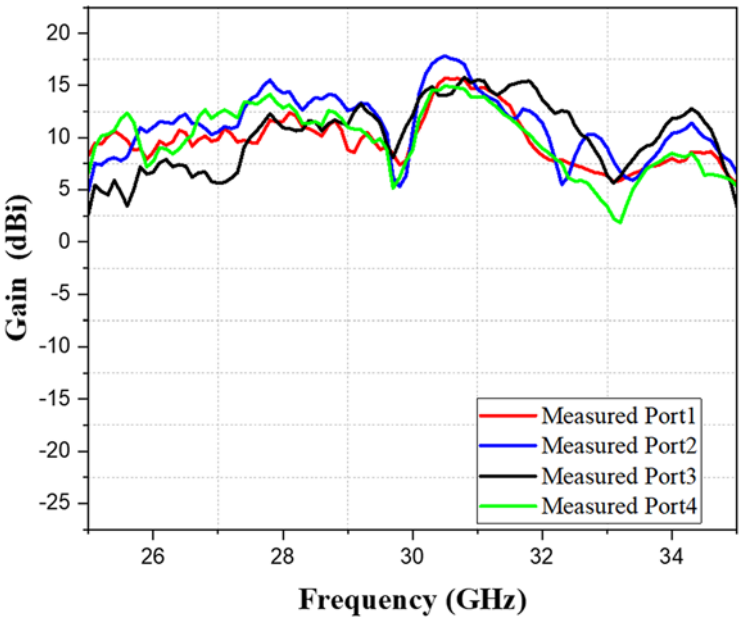

Figure 27. The measured gain of a sample of the Butler matrix antenna.

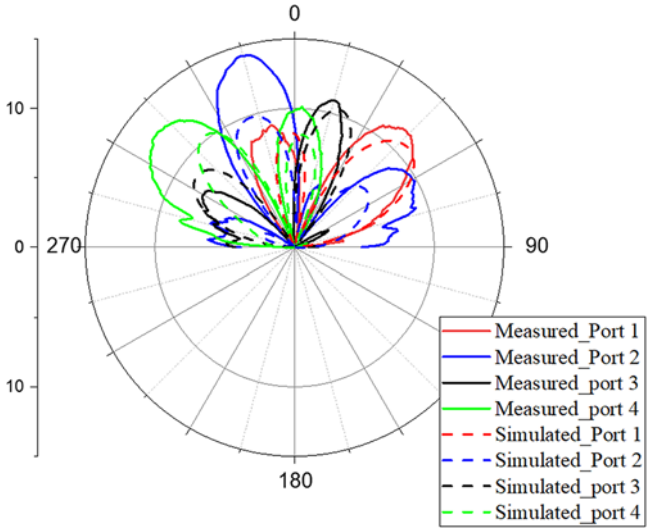

Figure 28. The measured and simulated beam angle of the Butler matrix antenna.

https://doi.org/10.1017/S1759078724001284 Published online by Cambridge University Press

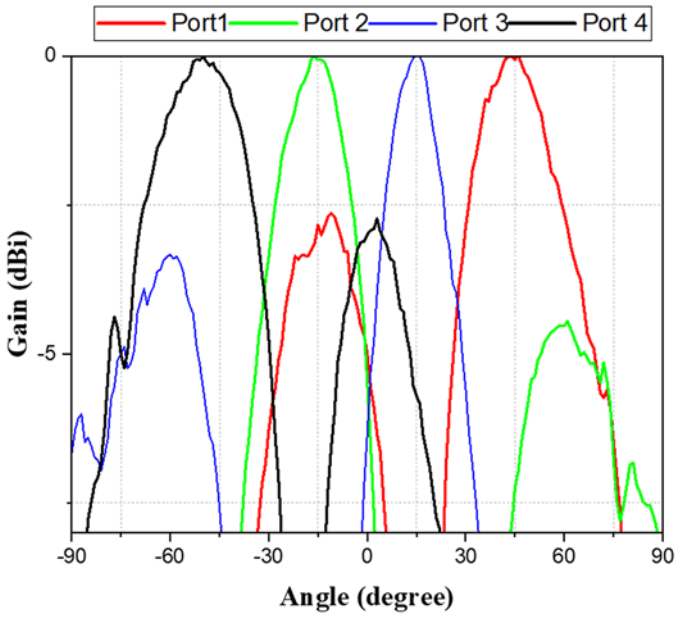

Figure 29. Normalized beam coverage of the Butler matrix antenna in the azimuth plane at a frequency of 28 GHz.

Table 3. Antenna comparison table for samples and other studies

Ref.	Freq. (GHz)	Size (mm)	Peck gain (dB)	Layers	Beam
[7]	24–28	N/A	9.5	Multiple	2×2
[8]	28	23.26 × 28.92	N/A	Single	4×4
[11]	28–32	53.6 × 15.8	10.2	Single	3×3
[12]	27–29	36 × 48	6.7	Single	4×4
[13]	28–32	56.5 × 21	11.2	Single	4×4
[14]	28–32	106 × 31.8	13.4	Single	6×6
[15]	28	90 × 45 × 11	14.1	Single	4×4
[16]	26–30	N/A	5.6	Multiple	4×4
[17]	24–28	≈150 × 160	12	Single	4×4
[18]	23.75–31	21.4 × 46	12.3	Multiple	4×4
[19]	27.8–30.8	Length ≈ 130	14.37	Multiple	5×8
[20]	26.5–32	Length ≈ 130	15.81	Multiple	8×8
[21]	28	101.6 × 63	6.1	Multiple	5×6
[22]	26	16 × 16	9.4 ∼ 10.9	multiple	16×16
[23]	28 ∼ 32	110.28 × 42.5	9.7 ∼ 12	Single	4×4
[24]	10	269 × 66		Single	3×3
[26]	35–41	36.9 × 16.3	7 ∼ 8	Single	4×4
Thiswork	≈26–32	56.8 × 21.2	14.28	Single	4×4

Conclusion

In this study, it is suggested that when designing an SIW Butler matrix, it may be beneficial to combine all the designed units (hybrid couplers, cross couplers, −90-degree phase shifter, and 0-degree phase shifter), connect the SIW transmission units and coaxial connectors, and then adjust the SIW transmission units to achieve the desired bandwidth. This method allows for a more streamlined design process and potentially better performance in terms of bandwidth and gain.

The proposed antenna in this paper achieves significant miniaturization and high gain. By adjusting the positions of the metal vias inward or adding an additional row of metal vias inside the existing ones without expanding the outer dimensions, the design addresses the issue of excessive dielectric loss leading to reduced radiation. This approach not only simplifies the structure but also makes it easy to fabricate, offering practical advantages for large-scale production and commercial applications.

https://doi.org/10.1017/S1759078724001284 Published online by Cambridge University Press

However, the proposed antenna still has the problem of high sidelobe levels. This issue remains an area for future research to find a reasonable solution under similar architectures. Despite this, the results suggest that the designed sample in this study exhibits favorable characteristics, with a broader bandwidth, compact size, and competitive gain performance when compared to other research designs.

In conclusion, the detailed examination and combination of Butler matrix units provided in this study offer valuable insights for future researchers. It is recommended that in the initial design phase of SIW Butler matrices, all units should be combined, and SIW transmission units and coaxial connectors should be connected. Following this, adjustments to the SIW transmission units should be made to achieve the desired bandwidth. Finally, verifying whether the beam angles align with the theoretical values will expedite the design process of SIW-type Butler matrices. The proposed design and methodologies discussed in this paper present a promising direction for the development of efficient and practical SIW Butler matrices and slot array antennas.

Data availability statement. All data are included within the manuscript.

Funding statement. This work was supported by the National Science and Technology Council, Taiwan, R.O.C., under Grant NSTC 113-2221-E-027-068.

Competing interests. The authors declare no conflict of interest.

References

1. **Chi L, Weng Z, Qi Y and Drewniak JL** (2020) A 60 GHz PCB wideband antenna-in-package for 5G/6G applications. *IEEE Antennas and Wireless Propagation Letters* **19**(11), 1968–1972. doi:10.1109/LAWP.2020.3006873
2. **Brandão T and Cerqueira A** (2022) Tri-band antenna array for FR1/FR2 5G NR base stations. *IEEE Antennas and Wireless Propagation Letters*.
3. **Tang Y, Dananjayan S, Hou C, Guo Q, Luo S and He Y** (2021) A survey on the 5G network and its impact on agriculture: Challenges and opportunities. *Computers and Electronics in Agriculture* **180**, 105895. doi:10.1016/j.compag.2020.105895
4. **Shallah AB, Zubir F, Rahim MKA, Majid HA, Sheikh UU, Murad NA and Yusoff Z** (2022) Recent developments of Butler matrix from components design evolution to system integration for 5G beamforming applications: A survey. *IEEE Access* **10**, 88434–88456. doi:10.1109/ACCESS.2022.3199739
5. **Acri G, Corsi J, Podevin F, Pistono E, Ferrari P and Boccia L** (2022) A sensitivity study of Butler matrices: Application to an SIW extended beam matrix at 28 GHz. *IEEE Access* **10**, 101972–101987. doi:10.1109/ACCESS.2022.3208055
6. **Shariff BP, Ali T, Mane PR and Kumar P** (2022) Array antennas for mmWave applications: A comprehensive review. *IEEE Access*.
7. **Xu Z, Shen Y, Xue S and Hu S** (2022) Fully planar 2-D multibeam millimeter-wave antenna with via-based phase shifters. *IEEE Antennas and Wireless Propagation Letters* **21**(11), 2234–2238. doi:10.1109/LAWP.2022.3195545
8. **Md Jizat N, Yusoff Z, Mohd Marzuki AS, Zainudin N and Yamada Y** (2022) Insertion loss and phase compensation using a circular slot via-hole in a compact 5G millimeter wave (mmWave) Butler matrix at 28 GHz. *Sensors* **22**(5), 1850. doi:10.3390/s22051850
9. **Vallappil AK, Rahim MKA, Khawaja BA, Murad NA and Mustapha MG** (2020) Butler matrix based beamforming networks for phased array antenna systems: A comprehensive review and future directions for 5G applications. *IEEE Access* **9**, 3970–3987. doi:10.1109/ACCESS.2020.3047696
10. **Wang J, Wu Y, Wang W and Ma L** (2022) Wideband mm-wave high-gain multibeam antenna array fed by 4× 4 groove gap waveguide Butler matrix with modified crossover. *AEU-International Journal of Electronics and Communications* **154**, 154287.
11. **Pezhman M, Heidari A and Ghafoorzadeh-Yazdi A** (2020) Compact three-beam antenna based on SIW multi-aperture coupler for 5G applications. *AEU-International Journal of Electronics and Communications* **123**, 153302.
12. **Lee S, Lee Y and Shin H** (2021) A 28-GHz switched-beam antenna with integrated Butler matrix and switch for 5G applications. *Sensors* **21**(15), 5128. doi:10.3390/s21155128
13. **Pezhman MM, Heidari -A-A and Ghafoorzadeh-Yazdi A** (2021) A compact 4× 4 SIW beamforming network for 5G applications. *AEU-International Journal of Electronics and Communications* **135**, 153714.
14. **Pezhman MM, Heidari -A-A and Ghafoorzadeh-Yazdi A** (2022) A novel single layer SIW 6× 6 beamforming network for 5G applications. *AEU-International Journal of Electronics and Communications* **155**, 154380.
15. **Najafabadi AMA, Ghani FA and Tekin I** (2022) Low-cost multi-beam millimeter-wave array antennas for 5G mobile applications. *IEEE Transactions on Vehicular Technology* **71**(12), 12450–12460. doi:10.1109/TVT.2022.3198878
16. **Wang D, Polat E, Tesmer H, Maune H and Jakoby R** (2022) Switched and steered beam end-fire antenna array fed by wideband via-less Butler matrix and tunable phase shifters based on liquid crystal technology. *IEEE Transactions on Antennas and Propagation* **70**(7), 5383–5392. doi:10.1109/TAP.2022.3142334
17. **Cao D, Li Y and Wang J** (2023) Ka-band multibeam patch antenna array fed by spoof-surface-plasmon-polariton Butler matrix. *IEEE Transactions on Antennas and Propagation* **71**(3), 2385–2395. doi:10.1109/TAP.2023.3240829
18. **Van Messem L, Moerman A, Caytan O, de Paula IL, Hoflack B, Stroobandt B, Lemey S, Moeneclaey M and Rogier H** (2022) A 4× 4 millimeterwave-frequency Butler matrix in grounded co-planar waveguide technology for compact integration with 5G antenna arrays. *IEEE Transactions on Microwave Theory & Techniques* **71**(1), 122–134. doi:10.1109/TMTT.2022.3178073
19. **Qin C, Chen F-C and Xiang K-R** (2021) A 5× 8 Butler matrix based on substrate integrated waveguide technology for millimeter-wave multi-beam application. *IEEE Antennas and Wireless Propagation Letters* **20**(7), 1292–1296. doi:10.1109/LAWP.2021.3078274
20. **Liu Z-P, Chen F-C and Qin C** (2022) A 7× 8 Butler matrix-fed multi-beam antenna based on substrate integrated waveguide technology. In *IEEE Antennas and Wireless Propagation Letters*.
21. **Han K, Wei G and Wang M** (2022) Design of millimeter wave dual-polarized multibeam antenna array with a boresight beam. *International Journal of RF and Microwave Computer-Aided Engineering* **32**(12), e23455. doi:10.1002/mmce.23455
22. **Kong W, Hu Y, Li J, Zhang L and Hong W** (2022) 2-D orthogonal multibeam antenna arrays for 5G millimeter-wave applications. *IEEE Transactions on Microwave Theory & Techniques* **70**(5), 2815–2824. doi:10.1109/TMTT.2022.3162113
23. **Yang Q-L, Ban Y-L, Lian J-W, Yu Z-F and Wu B** (2016) SIW Butler matrix with modified hybrid coupler for slot antenna array. *IEEE Access* **4**, 9561–9569. doi:10.1109/ACCESS.2016.2645938
24. **Wang Z, Dai X and Sun W** (2020) Tri-beam slot antenna array based on substrate integrated waveguide (SIW) technology. *International Journal of Microwave and Wireless Technologies* **12**(3), 246–251. doi:10.1017/S1759078719001260
25. **Mohan M, Hong MKC, Alphones A and Liu A** (2020) A 30 GHz SIW based 4×4 Butler matrix. In: *2020 IEEE International Symposium on Antennas and Propagation and North American Radio Science Meeting*. IEEE.
26. **Tsao Y-F, Hsu H-T and Desai A** (2023) High power handling GaAs SP4T switch-based beam-switching planar antenna module for 5G new-radio FR2 applications. *AEU-International Journal of Electronics and Communications* **159**, 154494.
27. **Desai A, Tsao Y-F and Hsu H-T** (2023) High gain substrate integrated waveguide antenna with enhanced bandwidth for millimeter-wave wireless network applications. *Wireless Networks* **29**(5), 2251–2260. doi:10.1007/s11276-023-03296-7

Ming-An Chung received the B.Eng. and M.Eng. degrees in electronic engineering from the Chang Gung University, Taoyuan, Taiwan and the D.Eng. degree in electrical engineering from the National Taiwan University of Science and Technology (NTUST), Taipei, Taiwan, in 2003, 2005, and 2016, respectively. He is currently an Associate Professor with the Department of Electronic Engineering, National Taipei University of Technology (NTUT), where he also serves as the Leader of the Innovation Wireless Communication and Electromagnetic Applications Laboratory. His research interests include wireless communication propagation, intelligent robotics, self-driving vehicles, antenna design for various mobile and wireless communications, electromagnetic theory, and applications. He is also a Reviewer of many scientific journals, including the IEEE TRANSACTIONS ON ANTENNAS AND PROPAGATION, IEEE Transactions on Industrial Informatics, Journal of Intelligent & Robotic Systems, IET Microwaves, Antennas and Propagation, IEEE Antennas and Wireless Propagation Letters, International Review of Electrical Engineering, International Journal on Communications Antenna and Propagation and AEÜ - International Journal of Electronics and Communications, and many international conferences, including ICRA, ICCE-TW, RFIT, ICBEB, EMCAR, and SNSP.

Ming-Chang Lee received B.S. degrees from Taipei University of Marine Technology in 2009 and M.S. degrees from National Taipei University of Technology in 2023. His research interests include Composite material antenna design, switched-beam antenna system, MIMO antenna system, millimeter-wave antenna design, and phased array antenna.

Chia-Chun Hsu received the Associate degree in computer and communication engineering from Army Academy R.O.C., Taiwan, in 2015. Her current research interests include antennas, MIMO antenna system design, and AIOT, emotion recognition applications.

Chia-Wei Lin received his B.S. and M.S. degrees from Chung Yuan Christian University in 2007 and is currently pursuing a Ph.D. degree in Electrical Engineering at the National Taipei University of Technology. His research interests include wireless communication propagation research, antenna design, intelligent robotics research, and self-driving vehicle research, embedded systems, deep learning.

https://doi.org/10.1017/S1759078724001284 Published online by Cambridge University Press